

The multiwavelength study of the infrared dust bubble S51

Chuan Peng Zhang^{1,2,3} and Jun Jie Wang^{1,2}

¹ National Astronomical Observatories, Chinese Academy of Sciences, Beijing 100012, China
e-mail: zcp0507@gmail.com

² NAOC-TU Joint Center for Astrophysics, Lhasa 850000, China

³ Graduate University of the Chinese Academy of Sciences, Beijing 100080, China

Received —; accepted —

ABSTRACT

Aims. We investigate the environment of the infrared dust bubble S51 and search for evidence of triggered star formation in its surroundings.

Methods. We perform a multiwavelength study of the region around S51 with data taken from large-scale surveys: 2MASS, GLIMPSE, MIPS GAL, IRAS and MALT90. We analyze the spectral profile and the distribution of the molecular gas (^{13}CO , C^{18}O , HCN, HNC, HCO^+ , C_2H , N_2H^+ and HC_3N), and dust in the environment of S51. We use mid-infrared emission three-color image to explore the physical environment and GLIMPSE color-color diagram [5.8]-[8.0] versus [3.6]-[4.5] to search for young stellar objects and identify the ionizing star candidates.

Results. From a comparison of the morphology of the molecular gas and the Spitzer 8.0 μm emission, we conclude that the dust bubble is interacting with CO at a kinematic distance of 3.4 kpc. The bubble S51 structure, carried with shell and front side, is exhibited with ^{13}CO and C^{18}O emission. Both outflow and inflow may exist in sources in the shell of bubble S51. We discover a small bubble G332.646-0.606 ($R_{in} = 26''$, $r_{in} = 15''$, $R_{out} = 35''$ and $r_{out} = 25''$) located at the northwest border of S51. A water maser, methanol maser and IRAS 16158-5055 are located at the junction of the two bubbles. Several young stellar objects are distributed along an arc-shaped structure near S51 shell. They may represent a second generation of stars whose formation was triggered by the bubble expanding into the molecular gas.

Key words. infrared: stars — stars: formation — ISM: bubbles — HII regions

1. Introduction

Churchwell et al. (2006, 2007) detected and catalogued about 600 mid-infrared dust (MIR) bubbles between longitudes -60° and $+60^\circ$. The bubbles have bright 8.0 μm shells that enclose bright 24 μm interiors. IR dust bubbles may be produced by exciting O- and/or B-type stars, which locate inside the bubble. The UV radiation from exciting stars may heat dust and ionize the gas to form an expanding bubble shell (Watson et al. 2008), which is known as "collect and collapse" process. This process can trigger the massive star formation near the shell clumps. These bubbles present an important opportunity to study the interaction between HII regions and molecular clouds.

We select an IR dust bubble S51 from the catalog of Churchwell et al. (2006). S51 is a complete (closed ring) IR dust bubble centered on $l=332.673$, $b=-0.618$. It lies in the southern part of RCW106 (Mookerjea et al. 2004; Wong et al. 2008; Lo et al. 2009). The radius of the shell is $1.48'$ (1.47 pc), and the average thickness of the shell is $0.32'$ (0.32 pc), and the eccentricity of the ellipse is 0.82. These assume a distance of 3.4 kpc.

MALT90 is a pilot survey conducted with the Mopra Telescope in preparation for the Millimeter Astronomy Legacy Team Survey at 90 GHz (Foster et al. 2011). One of aims of this multimolecular line mapping in this work is to examine how different molecules correlate with each other and with bubble S51. The molecules selected include ^{13}CO , C^{18}O , HCN, HNC, HCO^+ , C_2H , N_2H^+ and HC_3N . ^{13}CO has an optical depth of 1 to 12 (Wong et al. 2008), but C^{18}O can provide optical depth and line profile information ($n_{\text{crit}} = 3 \times 10^3 \text{cm}^{-3}$). MALT90 emission traces dense gas, and each molecular transition provides slightly different information. For example, HCN ($n_{\text{crit}} = 2 \times 10^5 \text{cm}^{-3}$) traces high column density and is optical thick; HNC ($n_{\text{crit}} = 3 \times 10^5 \text{cm}^{-3}$) is prevalent in cold gas ($n_{\text{crit}} = 2 \times 10^5 \text{cm}^{-3}$); HCO^+ ($n_{\text{crit}} = 4 \times 10^5 \text{cm}^{-3}$) often shows infall signatures and outflow wings (Rawlings et al. 2004; Fuller et al. 2005); N_2H^+ ($n_{\text{crit}} = 4 \times 10^5 \text{cm}^{-3}$) is more resistant to freeze-out on grains than the carbon-bearing species (Bergin et al. 2001); HC_3N is a good tracer of hot core chemistry.

In this work, we report a multiwavelength study of the environment surrounding the IR dust bubble S51. We aim to explore its surrounding ISM and search for signatures of star formation. We describe the data used in Sect.2; the results and discussion are presented in Sect.3; Sect.4 summarizes the results.

2. Data

We analyzed IR and millimeter wavelength data extracted from following large-scale surveys: the Two Micron All Sky Survey (2MASS)¹ (Skrutskie et al. 2006), GLIMPSE (Benjamin et al. 2003; Churchwell et al. 2009), MIPS GAL (Carey et al. 2009), IRAS (Neugebauer et al. 1984), and MALT90 (Foster et al. 2011).

GLIMPSE is a MIR survey of the inner Galaxy performed with the Spitzer Space Telescope. We used the mosaicked images from GLIMPSE and the GLIMPSE Point-Source Catalog (GPSC) in the Spitzer-IRAC (3.6, 4.5, 5.8 and $8.0 \mu\text{m}$). IRAC has an angular resolution between $1.5''$ and $1.9''$ (Fazio et al. 2004; Werner et al. 2004). MIPS GAL is a survey of the same region as GLIMPSE, using the MIPS instrument (24 and $70 \mu\text{m}$) on Spitzer. The MIPS GAL resolution is $6''$ at $24 \mu\text{m}$.

The Mopra 22-m radio Telescope has a full width at half maximum (FWHM) beam size of $\sim 33''$ at ~ 110 GHz for $^{13}\text{CO } J = 1-0$ and $\text{C}^{18}\text{O } J = 1-0$ transitions. The correlator was configured with 1024 channels over a 64-MHz bandwidth, which provided a velocity resolution of $\sim 0.17 \text{ km s}^{-1}$ per channel over a useable velocity bandwidth of $\sim 120 \text{ km s}^{-1}$ (Lo et al. 2009; Bains et al. 2006; Wong et al. 2008). The observing was set up so that the central channel corresponded to $\sim 50 \text{ km s}^{-1}$, at which the velocity of the emission from the GMC complex is centered.

¹ 2MASS is a joint project of the University of Massachusetts and the Infrared Processing and Analysis Center/California Institute of Technology, funded by the National Aeronautics and Space Administration and the National Science Foundation.

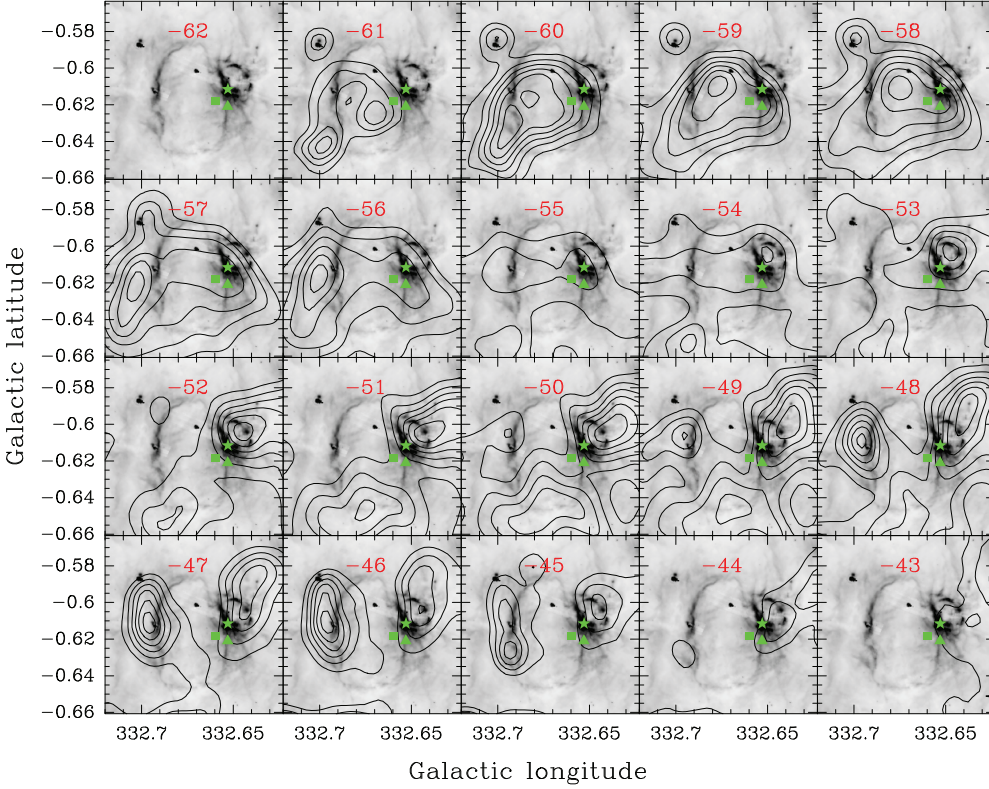


Fig. 1. Integrated velocity contours of the ^{13}CO emission every 1.0 km s^{-1} superimposing on the GLIMPSE $8.0 \mu\text{m}$ grayscale. The contours are at multiples of 13% level of each of the emission peaks. The peak of each mosaic from -62 to -43 km s^{-1} is 0.718, 1.632, 3.584, 7.503, 9.191, 11.388, 14.901, 16.428, 10.915, 9.673, 12.091, 15.416, 16.916, 16.467, 14.378, 12.772, 6.043, 3.018, 1.535 and $2.631 \text{ K km s}^{-1}$, respectively. The green symbols "▲", "■" and "★" indicate the positions of water maser, methanol maser and IRAS 16158-5055, respectively.

The On-The-Fly (OTF) mapping mode of Mopra was used for MALT90. Maps were made with the beam center running on a $3.4' \times 3.4'$ grid. The scan rate was $3.92''$ per second. The map is made with $12''$ spacing between adjacent rows, giving 17 rows per map. Since the Mopra beam at 90 GHz is $38''$, this row spacing provides redundancy in the map. The full 8 GHz bandwidth of Mopra Spectrometer (MOPS) was split into 16 zoom bands of 138 MHz each providing a velocity resolution of $\sim 0.11 \text{ km s}^{-1}$ in each band. In this work, six MALT90 Pilot Survey Lines (HCN ($J = 1 - 0$), HNC ($J = 1 - 0$), HCO^+ ($J = 1 - 0$), C_2H ($N = 1 - 0, J = 3/2 - 1/2, F = 2 - 1$), N_2H^+ ($J = 1 - 0$) and HC_3N ($J = 10 - 9$)) were used to trace the environment of bubble S51.

For the MOPRA observations, OFF positions were chosen at $\pm 1^\circ$ in Galactic latitude away from the plane (positive offset for sources at positive Galactic latitude and vice-versa), and a single OFF position was observed for every two scan rows. Pointing on SiO masers was performed every 1-1.5 hour, maintaining pointing precision to better than about $10''$. The brightness temperature T_{MB} is related to the antenna temperature T_A^* by $T_{MB} = T_A^*/\eta_\nu$, where η_ν is the frequency-dependent beam efficiency. According to Ladd et al. (2005) and Lo et al. (2009), the main beam efficiency at 86 GHz is $\eta_{86\text{GHz}} = 0.49$, and at 110 GHz is $\eta_{110\text{GHz}} = 0.44$. The results presented in this paper are in terms of main bright temperature $T_{MB}(\text{K})$. The ^{13}CO and C^{18}O data cubes were obtained from

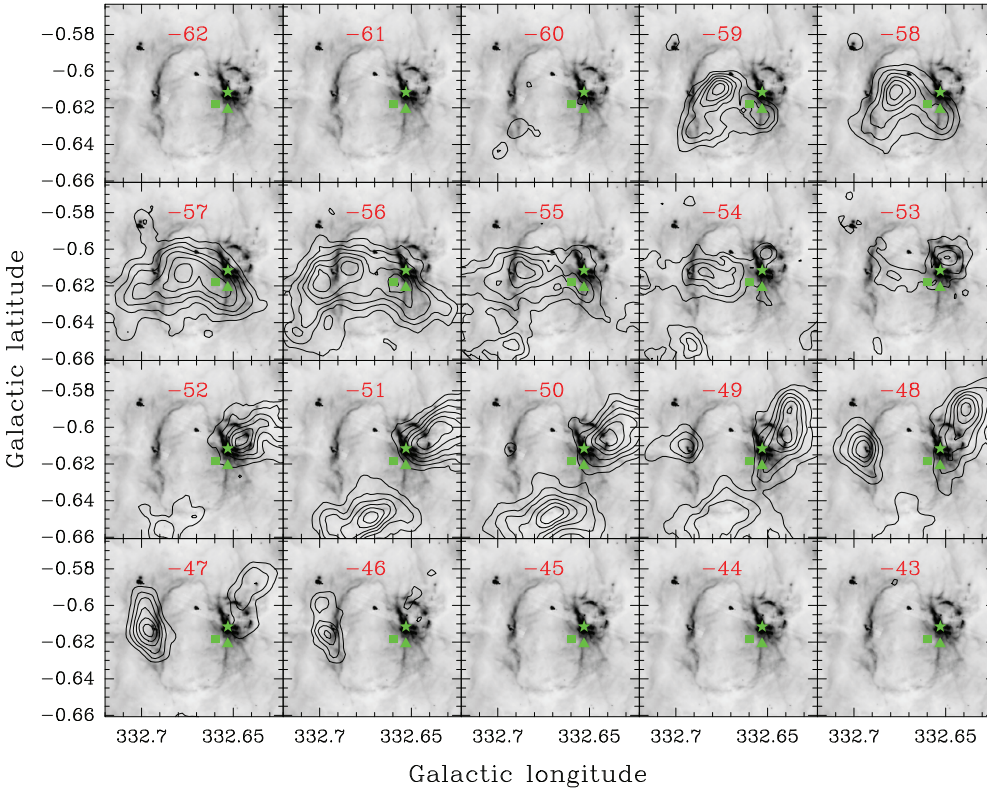


Fig. 2. Integrated velocity contours of the C^{18}O emission every 1.0 km s^{-1} superimposing on the GLIMPSE $8.0 \mu\text{m}$ grayscale. The contours are at multiples of 13% level of each of the emission peaks. The peak of each mosaic from -62 to -43 km s^{-1} is $0.518, 0.590, 0.870, 2.625, 4.342, 4.081, 3.663, 2.814, 1.627, 1.529, 2.671, 3.697, 4.914, 4.572, 4.514, 3.756, 1.524, 0.575, 0.558$ and $0.685 \text{ K km s}^{-1}$, respectively. The green symbols "▲", "■" and "★" indicate the positions of water maser, methanol maser and IRAS 16158-5055, respectively.

Lo et al. (2009). MALT90 data cubes were downloaded from online archive². The ^{13}CO , C^{18}O and MALT90 data cubes were processed with CLASS and GREG in GILDAS software package³.

3. Results and discussion

The clue of this section is as follows. Firstly, by analyzing the channel maps (Figs.1 and Fig.2) of bubble S51 with ^{13}CO and C^{18}O emission, we find that bubble S51 has shell and front side characters greatly associated with $8.0 \mu\text{m}$ emission. The integration intensity maps of $[-62.0 -43.]$, $[-62.0 -53.0]$ and $[-53.0 -43.0]$ components are shown in Fig.3. In addition, in order to examine the clumps of bubble S51, we use MALT90 multimolecular line mapping (Fig.A.1 in Appendix A) to compare with each other and with IR emission distribution. The molecules include HCN, HNC, HCO^+ , C_2H , N_2H^+ and HC_3N . And we also exhibit the spectra of these molecules in Fig.4. These spectra indicate that there are signs of inflow or outflow, whose velocity channels are shown in Fig.5. Furthermore, we exhibit two three-color images of MIR emission of IR dust bubble S51 with $3.6-4.5-8.0 \mu\text{m}$ and $4.5-8.0-24 \mu\text{m}$ in Fig.6, so that we can understand the IR structure of bubble S51. Finally, we use GLIMPSE color-color diagram $[5.8]-[8.0]$ versus $[3.6]-[4.5]$ (Fig.7)

² <http://atoa.atnf.csiro.au/MALT90/>

³ <http://iram.fr/IRAMFR/GILDAS/>

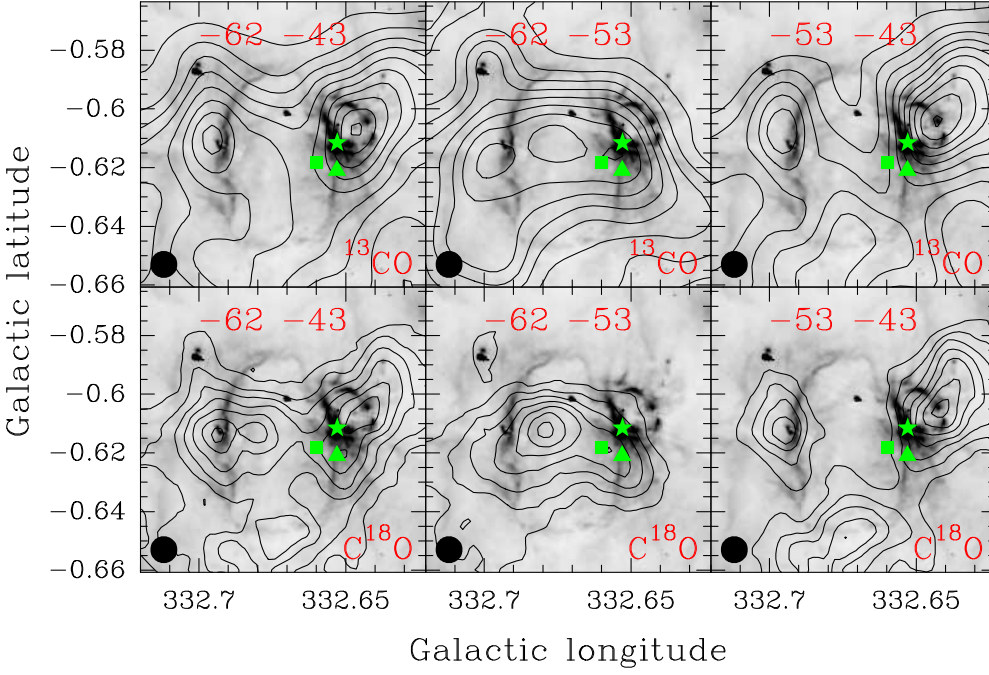


Fig. 3. Integrated velocity contours of the ^{13}CO (Upper three mosaics) and C^{18}O (Lower three mosaics) emission superimposing on the GLIMPSE $8.0\ \mu\text{m}$ grayscale. The contours are at multiples of 9% and 12% level of each of the ^{13}CO and C^{18}O emission peaks, respectively. The peaks of upper three mosaics from left to right are 123.136, 59.055 and 93.380 K km s^{-1} ; the peaks of lower three mosaics from left to right are 25.598, 18.456 and 20.458 K km s^{-1} , respectively. The integrated velocity range has been indicated in each panel. The green symbols "▲", "■" and "★" indicate the positions of water maser, methanol maser and IRAS 16158-5055, respectively.

and spectral energy distribution (SED) fitting (Fig.8) to search for young stars and identify exciting star candidate, whose distribution is shown in Fig.9.

3.1. The shell and front side of bubble S51

We inspected the molecular gas around S51 from the Mopra ^{13}CO and C^{18}O emission in the whole velocity range and found two independent velocity components ($[-62.0\text{--}53.0]$ and $[-53.0\text{--}43.0]$ km s^{-1}) along the line of sight. Fig.1 and Fig.2 show the integrated velocity maps of the ^{13}CO and C^{18}O emission every $1.0\ \text{km s}^{-1}$ between -62.5 and $-42.5\ \text{km s}^{-1}$. The $8.0\ \mu\text{m}$ grayscale shows the position and size of S51.

Comparing the molecular and MIR morphologies, there are many interesting places among the $[-62.0\text{--}53.0]$, $[-53.0\text{--}43.0]$ km s^{-1} components and $8.0\ \mu\text{m}$ emission, shown in Figs.1, 2 and 3. The morphology and peaks of $[-53.0\text{--}43.0]$ km s^{-1} component clearly correlate with $8.0\ \mu\text{m}$ emission. So the $[-53.0\text{--}43.0]$ km s^{-1} component may be the shell of bubble S51. On the other hand, looking at $-58.0\ \text{km s}^{-1}$ panel in Fig.2, we find that the contours fit quite well within the $8.0\ \mu\text{m}$ emission ring. Integration velocity map of $[-62.0\text{--}53.0]$ km s^{-1} component in Fig.3 also shows that there are good correlation between C^{18}O contours and $8.0\ \mu\text{m}$ emission. We suggest that this cloud could be blue shifted gas associated with the front side of bubble S51. Since the $-48.0\ \text{km s}^{-1}$ cloud is well

associated with bubble shell, this bubble would be expanding at roughly 10.0 km s^{-1} along the line of sight. However, there is no red shifted counterpart.

From the ^{13}CO and C^{18}O spectra of Fig.4, we also can see that there are two velocity components at the locations of sources A, B and C (see Fig.9), where source A is the core of eastern lobe of S51, source B lies at the front side or inside S51 and source C is the core of western lobe of S51. It is obvious that the spectral intensity of $[-62.0 -53.0] \text{ km s}^{-1}$ component at the front side of bubble is stronger than that of $[-53.0 -43.0] \text{ km s}^{-1}$. At the shell of bubble S51, however, it is just the reverse. This case is also the evidence of bubble S51 having shell and front side structure.

For $[-53.0 -43.0] \text{ km s}^{-1}$ component, the optical thin C^{18}O emission contours and spectra (Fig.2 and 4) show that the systematic velocity is $\sim -50.0 \text{ km s}^{-1}$. According to the galactic rotation model of Fich et al. (1989) (with $R_{\odot} = 8.5 \text{ kpc}$ and $\Theta_{\odot} = 220 \text{ km s}^{-1}$), we obtain kinematic distances of either 3.4 or 11.7 kpc. Lockman (1979) suggested that RCW106 lies the near kinematic distance after examining H_2CO absorption spectra seen against the HII region continuum. So, we adopt the near kinematic distance of 3.4 kpc in this work.

3.2. Opacity, excitation temperature and column density

We used the approach of Wong et al. (2008) to derive the opacity, excitation temperature and column density of ^{13}CO and C^{18}O within the box shown in Fig. A.1 of Appendix A. The size of the box is $4.3' \times 4.3'$ (where $4.3'$ is the diameter of S51). The velocity range included is just $V = \sim -53.0$ to $\sim -43.0 \text{ km s}^{-1}$ of bubble shell, and the box is centered on $l=332.673$, $b=-0.618$.

The relation between opacities and the ratio of ^{13}CO to C^{18}O main-beam brightness temperature (Myers et al. 1983) is

$$\frac{T_{MB}(^{13}\text{CO})}{T_{MB}(\text{C}^{18}\text{O})} = \frac{1 - \exp(-\tau_{13})}{1 - \exp(-\tau_{18})} = \frac{1 - \exp(-7.4\tau_{18})}{1 - \exp(-\tau_{18})}. \quad (1)$$

Equation (1) assumes $\tau_{13} = 7.4\tau_{18}$ (Wilson & Rood 1994; Wong et al. 2008). Furthermore, the excitation temperature T_{ex} is derived from the equation of radiative transfer:

$$\begin{cases} T_{MB} = f[J(T_{ex}) - J(T_{bg})][1 - \exp(-\tau)] \\ J(T) = T_0 / [\exp(T_0/T) - 1] \end{cases}, \quad (2)$$

where f is the beam filling factor, $T_{bg} = 2.7 \text{ K}$ and $T_0 = hv/k = 5.29 \text{ K}$ for the 1-0 transition of ^{13}CO (Wong et al. 2008). And then, assuming ^{13}CO is optical thin, we get the molecular ^{13}CO column density $N(^{13}\text{CO})$ from the relation (Bourke et al. 1997):

$$N(^{13}\text{CO})_{thin} = \frac{T_{ex} + 0.88}{1 - \exp(-5.29/T_{ex})} \cdot \frac{2.42 \times 10^{14}}{J(T_{ex}) - J(T_{bg})} \int T_{MB}(^{13}\text{CO}) dv. \quad (3)$$

Finally, assuming $[\text{H}_2/^{13}\text{CO}]$ abundance ratio is 7×10^5 (Frerking et al. 1982), the molecular hydrogen column $N(\text{H}_2)$ is then calculated. And then, the molecular cloud mass is estimated at $M_{shell} \sim 1.3 \times 10^4 M_{\odot}$ for bubble shell at a distance of $D_{S51} \sim 3.4 \text{ kpc}$.

3.3. Clump analysis

In order to examine the clumps of bubble S51, we used multimolecular line mappings to compare with each other and with IR emission distribution.

In the box shown in Fig. A.1, the maximum and average column densities $N(^{13}\text{CO})$ are 9.72×10^{17} and $5.98 \times 10^{16} \text{ cm}^{-2}$, respectively. This figure also shows the main beam brightness

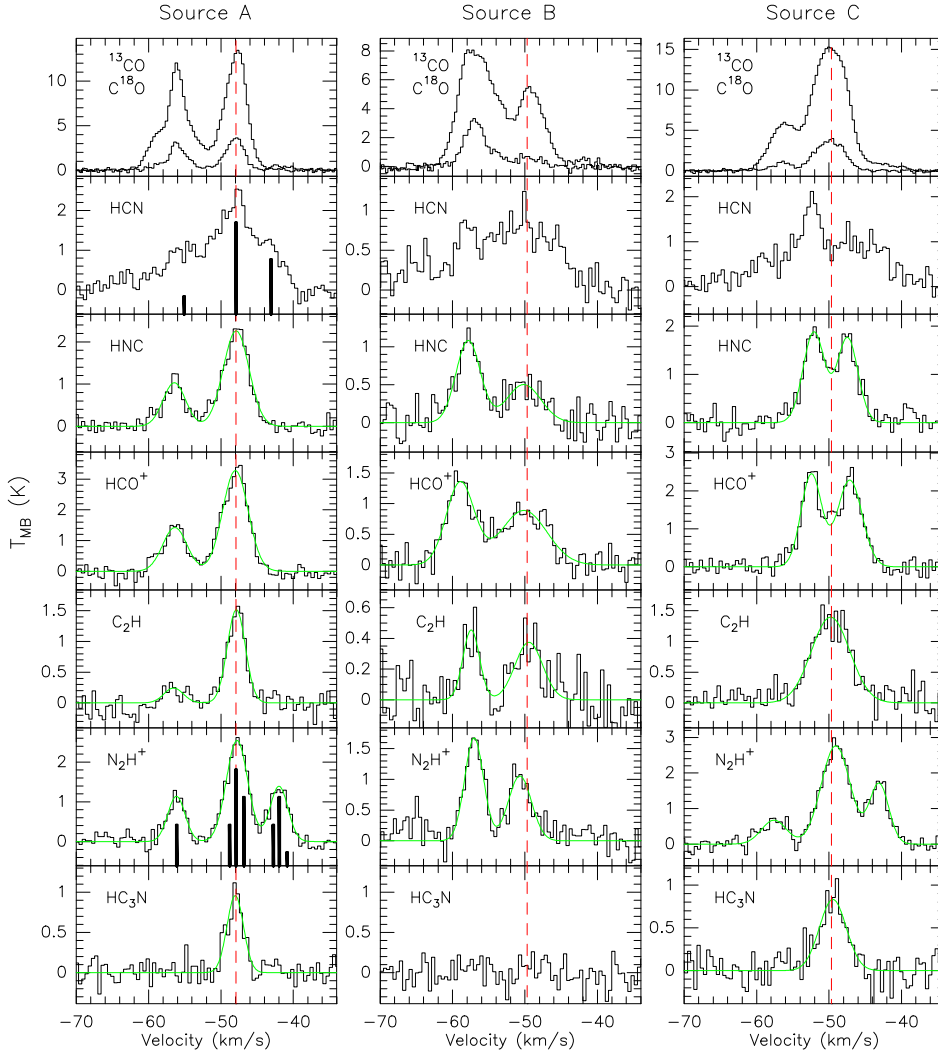


Fig. 4. MALT90 spectra of Source A, Source B and Source C, the position of which are represented in Fig.9 with "A" ($l=332.693, b=-0.610$), "B" ($l=332.677, b=-0.619$) and "C" ($l=332.645, b=-0.608$), respectively. The red dashed lines indicate the peak velocities of the $C^{18}O$ emission. The green curves are gauss-fit lines. HCN and N_2H^+ have hyperfine splitting, shown in black bar.

temperature T_{MB} , brightness temperature ratio $T_{MB}(^{13}CO)/T_{MB}(C^{18}O)$, optical depth $\tau(^{13}CO)$ and excitation temperature $T_{ex}(^{13}CO)$. The distribution of these parameters (shown in color) are compared with contours showing the integrated intensity of different molecular transitions. The average $T_{MB}(^{13}CO)/T_{MB}(C^{18}O)$, $\tau(^{13}CO)$ and $T_{ex}(^{13}CO)$ are 4.49, 1.76 and 20.91, respectively. The peak positions of ^{13}CO , $C^{18}O$ and $8.0 \mu m$ emission are spatially coincident, and situated at the east and west edge of the shell. And the molecular clouds are extended around the $8.0 \mu m$ emission peaks. At the south border of bubble S51, we also can see the shell of filament structure from $8.0 \mu m$ emission in Fig.6. The ^{13}CO and $C^{18}O$ emission contours are distributed along the shell of filament structure in Fig.3. We also see from Fig.A.1 that the distribution of $T_{MB}(^{13}CO)/T_{MB}(C^{18}O)$, $\tau(^{18}CO)$, $T_{ex}(^{13}CO)$ and $N(^{13}CO)$ shows an arc-like morphology around the north edge of S51. However, it should be noted that these derived properties are not independent of each other.

HCN, HNC, HCO^+ , C_2H and N_2H^+ trace the position of highest density, while HC_3N traces the location of hot core (Foster et al. 2011). We choose three sources (A, B and C) to analyze in

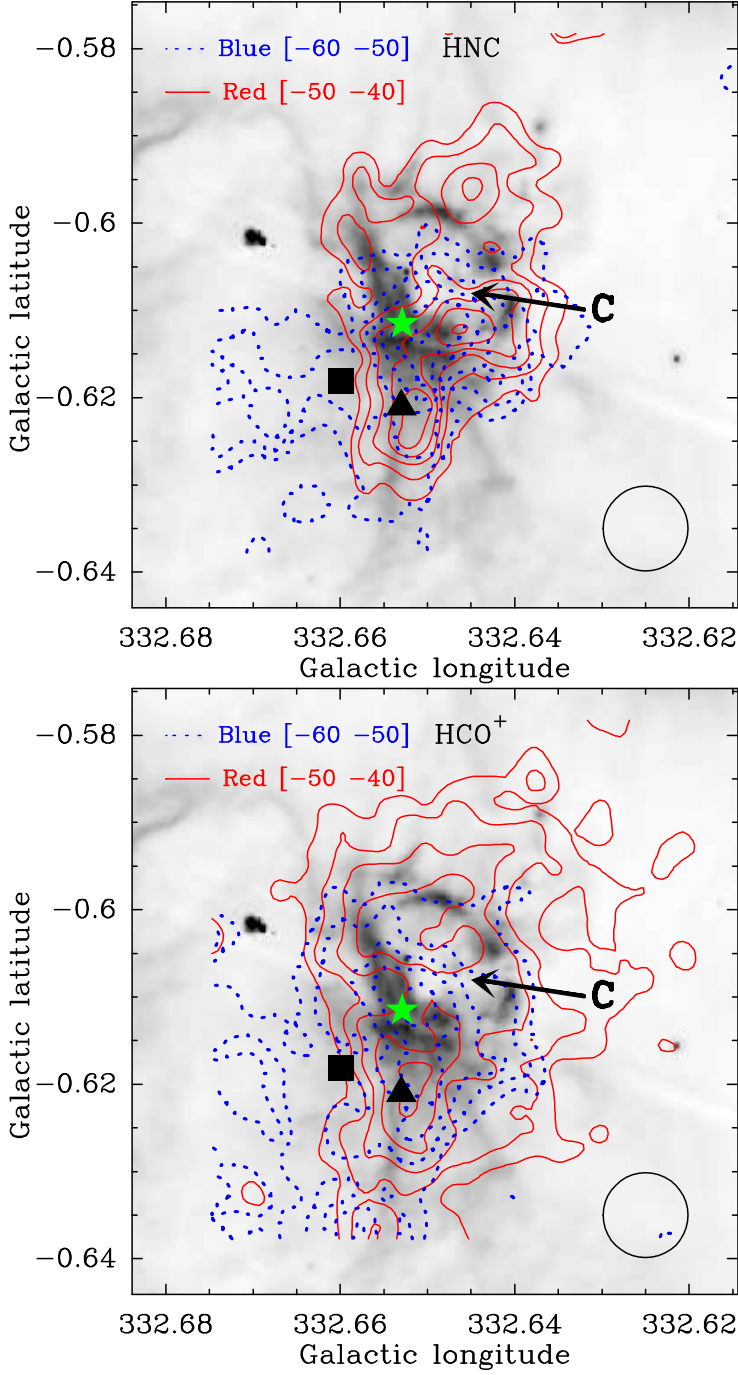


Fig. 5. Integrated velocity contours of HNC (Top panel) and HCO⁺ (Bottom panel) emission superimposing on the GLIMPSE 8.0 μm grayscale. The contours are at multiples of 11%, 11%, 12% and 12% level of each of the blue lobe of HNC, red lobe of HNC, blue lobe of HCO⁺, and red lobe of HCO⁺ emission peaks, which are 9.539, 8.618, 12.861 and 10.800 K km s⁻¹, respectively. Source C is indicated with "C" in the image. The symbols "▲", "■" and "★" indicate the positions of water maser, methanol maser and IRAS 16158-5055, respectively.

Fig.9; spectra of them are shown in Fig.4. Fig.A.1 shows that an potential dense and hot core are mainly located in the eastern and western shells. The spectra shown in Fig.4 for the [-53.0 -43.0] km s⁻¹ component demonstrate that source B inside S51 has a lower brightness temperature than the sources A and C in S51 shell. At the source B, however, the MALT90 spectra of the [-53.0

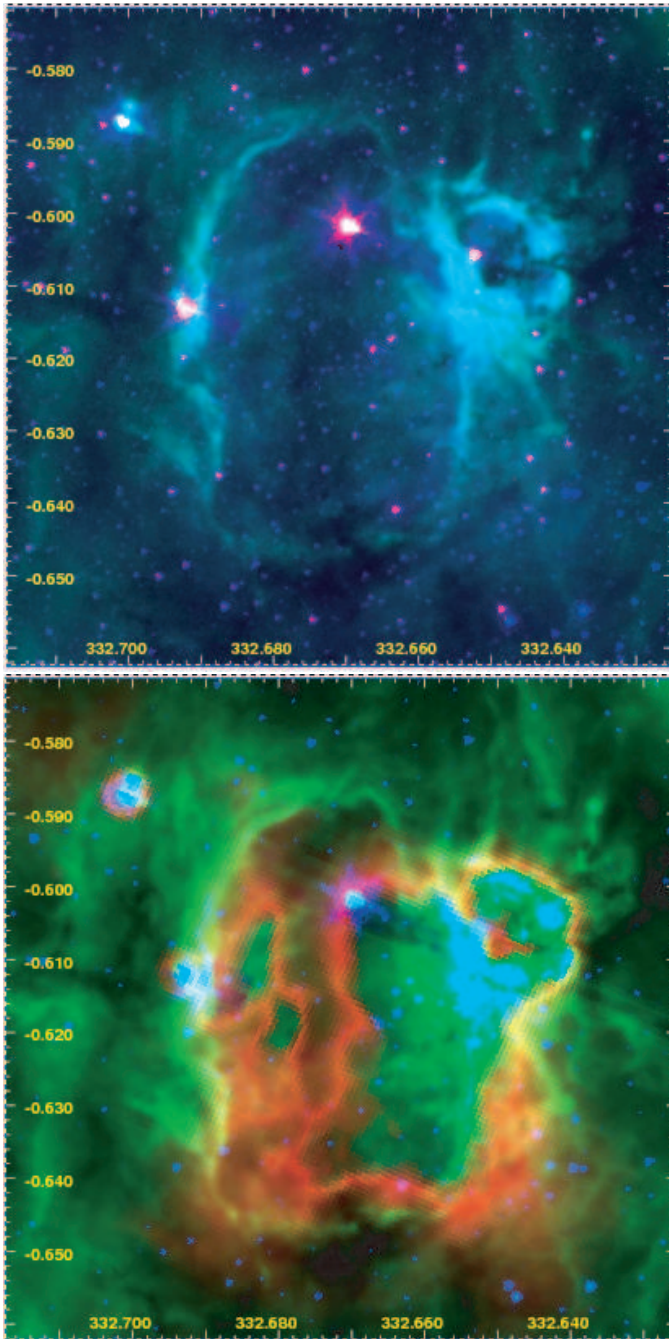


Fig. 6. MIR emission of IR dust bubble S51. *Top:* Spitzer-IRAC three-color image ($3.6\ \mu\text{m}$ = red, $4.5\ \mu\text{m}$ = blue and $8.0\ \mu\text{m}$ = green); *Bottom:* Spitzer-IRAC and Spitzer-MIPSGAL three-color image ($4.5\ \mu\text{m}$ = blue, $8.0\ \mu\text{m}$ = green and $24\ \mu\text{m}$ = red). Note that the $24\ \mu\text{m}$ emission is saturated at the center of image.

$-43.0]$ km s^{-1} component show the blueshifted velocity $[-62.0 -53.0]$ km s^{-1} , which is the evidence of having the front side of bubble S51. It is suggestive that the extended cloud of $[-53.0 -43.0]$ km s^{-1} component is scarce inside bubble S51, and the front side of bubble S51 has rich abundance. However, the back side of bubble S51 is not shown in MALT90 spectra. MALT90 spectra also show that bubble S51 might be expanding at $10\ \text{km s}^{-1}$ relative to bubble shell along the line of sight. In addition, we note IRAS 16158-5055 is closer to the peaks of N_2H^+ and HC_3N than the water maser and methanol maser.

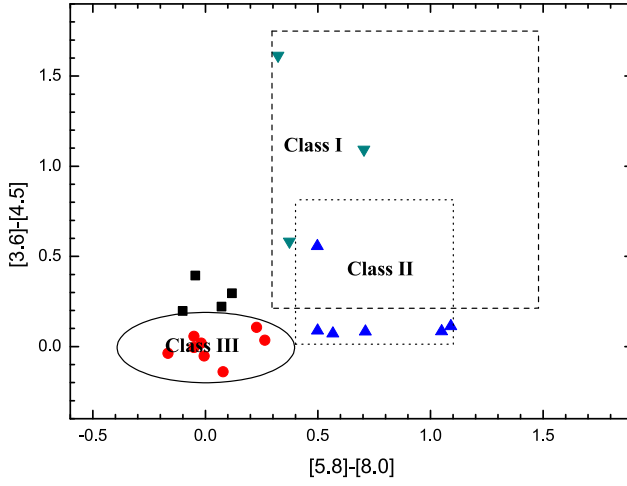


Fig. 7. GLIMPSE color-color diagram $[5.8]-[8.0]$ versus $[3.6]-[4.5]$ for sources in and around S51. The symbols "▼", "▲", "●" and "■" indicate the different stars of Class I, II, III and others, respectively. The classification of Class I, II and III indicates the stellar evolutionary stage as defined by Allen et al. (2004).

3.4. Inflow or outflow character

As shown in Fig.5, there is much trace of active star formation located in the shell of S51. The western shell of S51 contains a UCHII region, water maser ($l=332.653$, $b=-0.621$), methanol maser ($l=332.660$, $b=-0.618$) and IRAS 16158-5055 ($l=332.653$, $b=-0.612$) (Walsh et al. 1997; Breen et al. 2007). The water maser spectrum has three peaks, with fluxes of ~ 1 Jy for the -58.5 km s^{-1} component, ~ 6 Jy for -47.5 km s^{-1} and ~ 30 Jy for -45.2 km s^{-1} , respectively (Walsh et al. 1997). The methanol maser spectrum has a velocity range of $-52 \sim -50$ km s^{-1} , and the peak flux is 7.1 Jy (Breen et al. 2007). So, the $[-53.0 -43.0]$ km s^{-1} component of the S51, rather than the $[-62.0 -53.0]$ km s^{-1} component of background, is strongly correlated with the methanol and water masers.

On the west side of S51, the position of source C is marked in Fig.5. Fig.4 shows the ^{13}CO , C^{18}O and MALT90 spectra of source C. We mark the splittings of hyperfine structure of HCN and N_2H^+ with several black bars. The $[-62.0 -53.0]$ km s^{-1} component is very faint in ^{13}CO , C^{18}O emission, as well as HCN, HNC, HCO^+ , C_2H and HC_3N . So the $[-62.0 -53.0]$ km s^{-1} component seems unrelated to the $[-53.0 -43.0]$ km s^{-1} component in this cluster. Fig.4 also shows that the optical thick spectra of HCN, HNC and HCO^+ lines have absorption dips at the peak velocity (-49.5 km s^{-1}) traced by C^{18}O , C_2H , N_2H^+ and HC_3N . The blue profile is stronger than red profile shown from HCN spectrum. Such a profile can be produced by inflow with cold gas wings and a hot central core (Mardones et al. 1997). Moreover, HNC and HCO^+ have broad line wings corresponding to N_2H^+ and HC_3N , so source C could also be produced by outflow. Fig.5 shows the emission in two different velocity channels. The velocities of water maser and methanol maser are similar to the more negative velocity gas. We speculate that since this region is located at the junction of bubble S51 and bubble G332.646-0.606 (referred to Sect.3.5), it is plausible the interactions between two bubbles or between HII region and the molecular cloud have triggered this phenomenon.

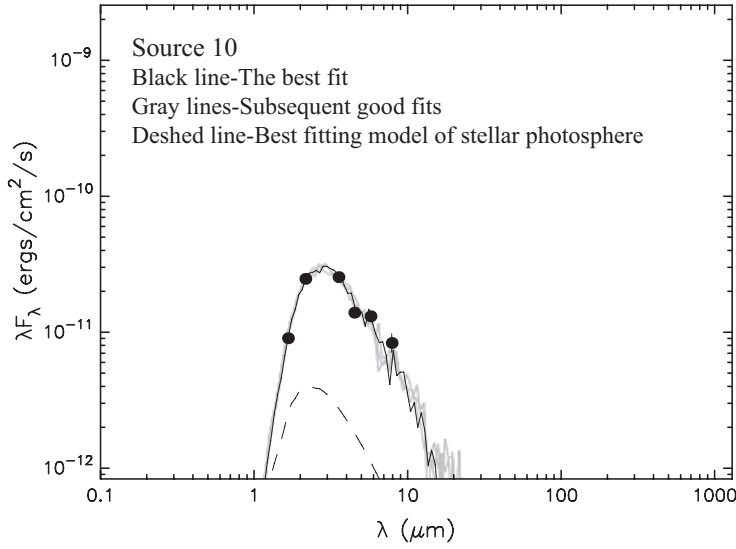


Fig. 8. The SED fits of exciting star source 10 ($l=332.6664$, $b=-0.6266$). The flux density of fitted data are 2Mass H-Band 5.01(0.22), K-Band 17.81(0.44), IRAC 3.6 μm 30.16(1.26), 4.5 μm 20.93(1.48), 5.8 μm 25.12(1.53), and 8.0 μm 22.15(3.46) mJy, respectively.

3.5. IR structure of S51

Fig.6 shows two Spitzer three-color images of S51. Both figures clearly show the PDR visible in 8.0 μm (in green) emission, which originates mainly in the PAHs. Since these large molecules are destroyed inside the ionized region, the PAH emission delineates the HII region boundaries, and the molecular clouds are excited in the PDR by the radiation leaking from the HII region (Petriella et al. 2010; Pomarès et al. 2009). The 24 μm emission (bottom panel in Fig.6), appears inside the bubble S51, and corresponds to hot dust. It is likely that O- and/or early B-type stars produced the bubble shell of this HII region, with hot dust located inside the bubble. The 3.6 μm emission (in red, top panel in Fig.6) shows the positions of the brightest stars.

We also note a small bubble G332.646-0.606, which is centered on $l=332.646$, $b=-0.606$ and located on the northwest edge of S51. The semimajor (R_{in}) and semiminor (r_{in}) axes of the inner ellipse are 26 and 15 arcsec, respectively; the semimajor (R_{out}) and semiminor (r_{out}) axes of the outer ellipse are 35 and 25 arcsec, respectively. From 8.0 μm emission of bubble G332.646-0.606, the elliptical morphologic PDR shows the sketch of bubble. Note that the 24 μm emission is saturated inside the small bubble G332.646-0.606. At the junction between bubble S51 and G332.646-0.606, the IR emission is brighter than the rest of the shell; this is also true for the ^{13}CO , C^{18}O and MALT90 emission lines. IRAS 16158-5055 is also located at this position. It seems likely that this junction region is the birth space of several YSOs. In addition, the molecular gas of the bubble shell exhibits several clumps along the PDR (Fig.6). The distribution and morphology of this material is suggestive that the collect and collapse process may be occurring.

3.6. Search for young stars and identify exciting stars

The distribution of IR point sources in the surroundings of S51 provides some signs of star formation. Fig.7 shows the [5.8]-[8.0] versus [3.6]-[4.5] color-color diagram for the sources extracted from the GLIMPSE Point Source Catalog in the Spitzer-IRAC bands in and around S51. We only

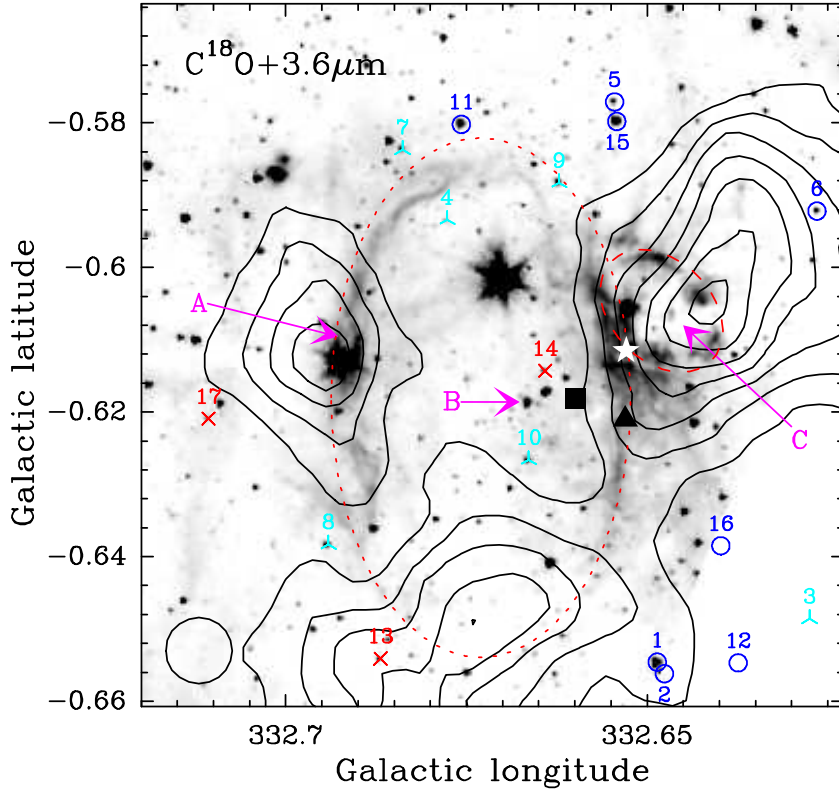


Fig. 9. Integrated velocity contours of the ^{18}CO emission superimposing on the GLIMPSE $3.6\ \mu\text{m}$ grayscale. The contours are at multiples of 12% level of the C^{18}O emission peaks $93.380\ \text{K km s}^{-1}$, and the integrated velocity range is from -53.0 to $-43.0\ \text{km s}^{-1}$. Two dashed ellipses show the PAH morphology of two bubbles. Letters "A" ($l=332.693$, $b=-0.610$), "B" ($l=332.677$, $b=-0.619$) and "C" ($l=332.645$, $b=-0.608$) give the chosen positions of three sources. The class I, II and III stars are indicated with symbols "x", " λ " and "o". The symbols " \blacktriangle ", " \blacksquare " and " \star " indicate the positions of water maser, methanol maser and IRAS point source, respectively.

consider sources with detection in the four Spitzer-IRAC bands. In Fig.7, class I stars are protostar with circumstellar envelopes; class II are disk dominated objects; and class III are main sequence and giant stars. The classification indicates the stellar evolutionary stage as defined by Allen et al. (2004).

Class I and class II stars are chosen to be the YSO candidates. The YSO candidates are drawn with symbols "x" and " λ " in Fig.9, among which sources 4, 7, 8, 9, 13 and 17 near the shell of bubble make up of arc-shaped distribution. This may be caused by interaction between HII region and molecular clouds, and the production of collect and collapse process.

We also try to search and identify exciting stars of S51. However, only sources 10 and 14 are located within bubble. Source 14 belongs to class I star, so we do not consider it as exciting stars. Source 10 is class II star, so we will identify it further more with SED fitting, using the tool developed by Robitaille et al. (2007) available online⁴. The good fitting models are selected according to the condition $\chi^2 - \chi_{min}^2 < 3$, where χ_{min}^2 is the minimum value of χ^2 among all models.

In Fig.8, we show the results for our source 10 of SED fitting to the fluxes obtained from GLIMPSE Point Source Catalog (Hora et al. 2008) and 2MASS All-Sky Point Source Catalog

⁴ <http://caravan.astro.wisc.edu/protostars/>

(Skrutskie et al. 2006). We fit these sources allowing the extinction to range from 0 to 30 mag and the distance to range from 3.0 to 4.0 kpc. The SED output shows that source 10 in class II is $\dot{M}_{env}/M_{\star} < 10^{-6} \text{ yr}^{-1}$ and $M_{disk}/M_{\star} < 10^{-6}$; the temperature of center star is 31000 K, in agreement with the effective temperature expected for an O-type star (Schaerer & de Koter 1997). Therefore, source 10 may be a candidate of the ionization of S51. Stellar winds emit from exciting stars. In addition the presence of a central cavity in the distribution of the ionized gas may be a signature of the activities of stellar winds. The location of source 10 inside this cavity provides additional support for this star being the most likely candidate for creating S51. Spectroscopic observation is needed to confirm this.

4. Summary

We have investigated the environment of the IR dust bubble S51 with several spectra (^{13}CO , C^{18}O , HCN, HNC, HCO^+ , C_2H , N_2H^+ and HC_3N) and IR emission. The main results can be summarized as follows.

(1) We have distinguished two independent velocity components associated with S51 along the line of sight. One component belong to the shell of bubble S51, and another may be the front side of bubble S51.

(2) We suggest that Source C ($l=332.645$, $b=-0.608$) shows evidence of either outflow or inflow, located in the northwest border of S51.

(3) Next to the west border of bubble S51, we find a small bubble G332.646-0.606, whose dimensions are $R_{in} = 26''$, $r_{in} = 15''$, $R_{out} = 35''$ and $r_{out} = 25''$.

(4) MALT90 emission contours appear to be correlated with the S51 shell. Water maser, methanol maser and IRAS 16158-5055 are located in the shell. YSO distribution is also correlative with ^{13}CO , C^{18}O and $8.0 \mu\text{m}$ emission.

Acknowledgements. We wish to thank the anonymous referee for comments and suggestions which improved the clarity of the paper. Particularly, we thank Dr. Nadia Lo for providing ^{13}CO and C^{18}O data. This work was supported by the Young Researcher Grant of National Astronomical Observatories, Chinese Academy of Sciences No.O835032002.

References

- Allen, L. E., Calvet, N., D'Alessio, P., et al. 2004, *ApJS*, 154, 363
 Bains, I., Wong, T., Cunningham, M., et al. 2006, *MNRAS*, 367, 1609
 Benjamin, R. A., Churchwell, E., Babler, B. L., et al. 2003, *PASP*, 115, 953
 Bergin, E. A., Ciardi, D. R., Lada, C. J., Alves, J., & Lada, E. A. 2001, *ApJ*, 557, 209
 Bourke, T. L., Garay, G., Lehtinen, K. K., et al. 1997, *ApJ*, 476, 781
 Breen, S. L., Ellingsen, S. P., Johnston-Hollitt, M., et al. 2007, *MNRAS*, 377, 491
 Carey, S. J., Noriega-Crespo, A., Mizuno, D. R., et al. 2009, *PASP*, 121, 76
 Churchwell, E., Babler, B. L., Meade, M. R., et al. 2009, *PASP*, 121, 213
 Churchwell, E., Povich, M. S., Allen, D., et al. 2006, *ApJ*, 649, 759
 Churchwell, E., Watson, D. F., Povich, M. S., et al. 2007, *ApJ*, 670, 428
 Fazio, G. G., Hora, J. L., Allen, L. E., et al. 2004, *ApJS*, 154, 10
 Fich, M., Blitz, L., & Stark, A. A. 1989, *ApJ*, 342, 272
 Foster, J. B., Jackson, J. M., Barnes, P. J., et al. 2011, *ApJS*, 197, 25
 Frerking, M. A., Langer, W. D., & Wilson, R. W. 1982, *ApJ*, 262, 590
 Fuller, G. A., Williams, S. J., & Sridharan, T. K. 2005, *A&A*, 442, 949
 Hora, J. L., Carey, S., Surace, J., et al. 2008, *PASP*, 120, 1233

- Ladd, N., Purcell, C., Wong, T., & Robertson, S. 2005, *PASA*, 22, 62
- Lo, N., Cunningham, M. R., Jones, P. A., et al. 2009, *MNRAS*, 395, 1021
- Lockman, F. J. 1979, *ApJ*, 232, 761
- Mardones, D., Myers, P. C., Tafalla, M., et al. 1997, *ApJ*, 489, 719
- Mookerjea, B., Kramer, C., Nielbock, M., & Nyman, L.-Å. 2004, *A&A*, 426, 119
- Myers, P. C., Linke, R. A., & Benson, P. J. 1983, *ApJ*, 264, 517
- Neugebauer, G., Habing, H. J., van Duinen, R., et al. 1984, *ApJ*, 278, L1
- Petriella, A., Paron, S., & Giacani, E. 2010, *A&A*, 513, A44
- Pomarès, M., Zavagno, A., Deharveng, L., et al. 2009, *A&A*, 494, 987
- Rawlings, J. M. C., Redman, M. P., Keto, E., & Williams, D. A. 2004, *MNRAS*, 351, 1054
- Robitaille, T. P., Whitney, B. A., Indebetouw, R., & Wood, K. 2007, *ApJS*, 169, 328
- Schaerer, D. & de Koter, A. 1997, *A&A*, 322, 598
- Skrutskie, M. F., Cutri, R. M., Stiening, R., et al. 2006, *AJ*, 131, 1163
- Walsh, A. J., Hyland, A. R., Robinson, G., & Burton, M. G. 1997, *MNRAS*, 291, 261
- Watson, C., Povich, M. S., Churchwell, E. B., et al. 2008, *ApJ*, 681, 1341
- Werner, M. W., Roellig, T. L., Low, F. J., et al. 2004, *ApJS*, 154, 1
- Wilson, T. L. & Rood, R. 1994, *ARA&A*, 32, 191
- Wong, T., Ladd, E. F., Brisbin, D., et al. 2008, *MNRAS*, 386, 1069

Appendix A: Molecular Line maps of bubble S51

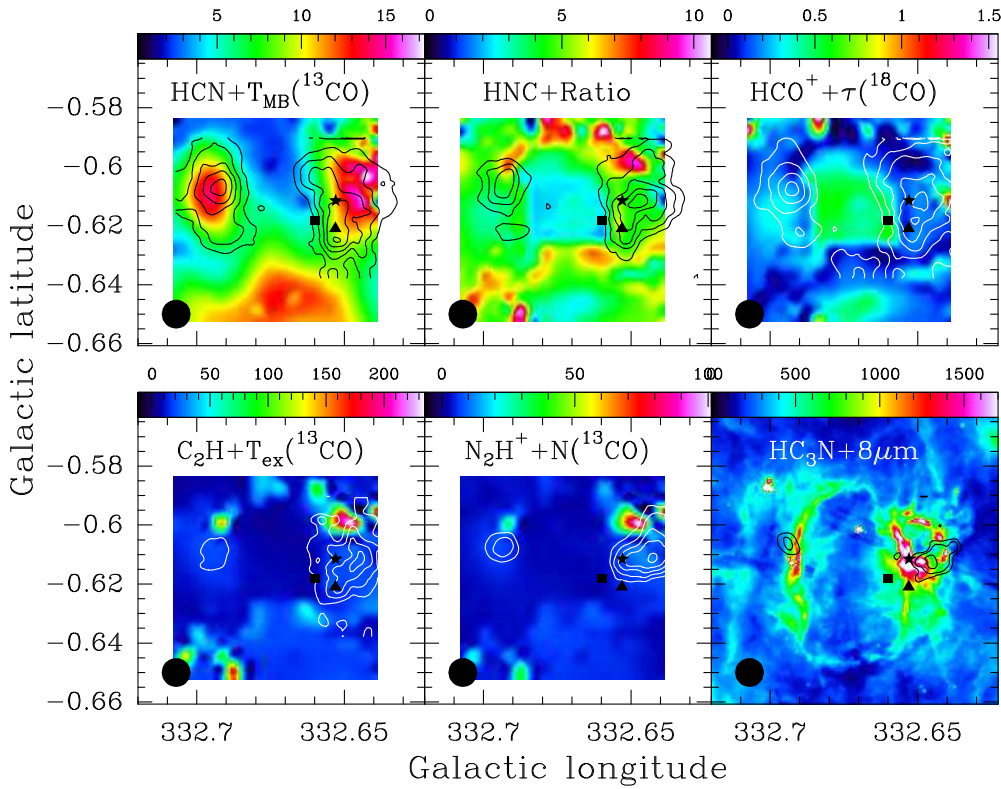


Fig. A.1. Integrated velocity contours of MALT90 emissions (HCN, HNC, HCO⁺, C₂H, N₂H⁺ and HC₃N) superimposing on six color images of different parameter distributions ($T_{MB}({}^{13}\text{CO})$, Ratio = $T_{MB}({}^{13}\text{CO})/T_{MB}(\text{C}^{18}\text{O})$, $\tau({}^{18}\text{CO})$, $T_{ex}({}^{13}\text{CO})$, $N({}^{13}\text{CO})[\times 10^{16}]$ and $8\ \mu\text{m}$). The contours are at multiples of 12%, 13%, 12%, 16%, 14% and 15% level of each of the HCN, HNC, HCO⁺, C₂H, N₂H⁺ and HC₃N emission peaks, which are 9.573, 7.953, 9.781, 4.791, 10.490 and 2.555 K km s⁻¹, respectively. The integrated velocity range is from ~ -53.0 to ~ -43.0 km s⁻¹ for all contours. The black symbols "▲", "■" and "★" indicate the positions of water maser, methanol maser and IRAS 16158-5055, respectively.